Bulletin of Engineering Geology and the Environment (2022) 81: 149
https://doi.org/10.1007/s10064-022-02614-1

ORIGINAL PAPER

Dynamic evolution mechanism and subsequent reactivated ancient landslide analyses of the "6.17" Danba sequential disasters

Nan Jiang[1] · Hai-bo Li[2] · Yu-xiang Hu[1] · Jie-yuan Zhang[2] · Wei Dai[1] · Cong-jiang Li[2] · Jia-wen Zhou[1]

Received: 20 June 2021 / Accepted: 15 February 2022 / Published online: 15 March 2022

Abstract
On June 17, 2020, a sequential disaster event, including debris flows, dammed lakes and the reactivation of ancient landslides, occurred in Danba County, Southwest China. The debris flow, which was triggered by short-term heavy rainfall, caused damage to houses and casualties, eventually leading to the blockage of the main channel of the Xiaojinchuan River as well as the formation of a debris flow–dammed lake. The outburst flood induced by the breakage of the debris flow dam caused devastating damage to dozens of villages, towns, and national highway G350 downstream. Moreover, an ancient landslide located on the left bank was reactivated during the outburst flood and experienced a large degree of deformation for several months. According to this sequential disaster event, we conducted on-site surveys and monitoring using three-dimensional terrestrial laser scanning (TLS) and unmanned aerial vehicles (UAVs). The development and dynamic evolution mechanism of the debris flow, dammed lake, and reactivated ancient landslide were illustrated based on the monitoring data. The results show that the erosion of outburst floods is the main cause of the deep and shallow sliding of the ancient landslide, and the presence of landslide deposits or unstable slopes near the debris flow dam sites is the key factor in the amplification and expansion of the disasters.

Keywords Debris flow · Dammed lake · Sequential disasters · Reactivation of an ancient landslide · Remote sensing technology

Introduction

Landslides, debris flows, dammed lakes, and other natural hazards often occur in the mountainous areas of Southwest China (Hu and Huang 2017). The topography of high alpine canyons provides favorable geographical conditions for the occurrence of geological hazards (Ge et al. 2017). In addition, the heavy rainfall in the flood season brings plenty of surface runoff and material sources for the formation of debris flows, landslides, collapses, and dammed lakes (Cui et al. 2013; Martha et al. 2015; Cai et al. 2020). Moreover, the occurrence and development of a natural disaster may not only cause damage to traffic and facilities but also trigger secondary disasters and form sequential disasters, resulting in an exponential increase in the scale and severity of natural disasters (Tacconi Stefanelli et al. 2018; Zhou et al. 2020b; Li et al. 2021; Shen et al. 2021). The typical forms of sequential disaster events include (a) debris flows formed on the landslide deposits under the effect of heavy rainfall (Samodra et al. 2018; Setiawan et al. 2019); (b) landslides that occur immediately above the river channels, leading to the formation of landslide-dammed lakes (Zygouri and Koukouvelas 2018; Brideau et al. 2019; Koukouvelas et al. 2020b); and (c) debris flows formed in the tributary channel entering the main channel, thereby blocking the main channel and forming debris flow–dammed lakes (Chen et al. 2019). Among these sequential disasters, the formation of a dammed lake and the ensuing outburst flood are the key contributors to the multiplication of disasters (Zou et al. 2013; Zhou et al. 2016). Because of the large amount of sands, gravels, rocks, and boulders, outburst floods during the break of a landslide dam or a debris flow dam drastically change the original river channel and cause severe damage to villages, towns, cities, and roads downstream (Yang et al. 2020). In addition, outburst floods can cause severe erosion to the riverbank and riverbed at the breach due to the strong incision during the flood peak.

On June 17, 2020, a sequential natural disaster event containing a debris flow, a dammed lake, and a reactivated ancient landslide occurred in Banshanmen town, Danba County,

✉ Jia-wen Zhou
jwzhou@scu.edu.cn

[1] State Key Laboratory of Hydraulics and Mountain River Engineering, Sichuan University, Chengdu 610065, People's Republic of China

[2] College of Water Resource and Hydropower, Sichuan University, Chengdu 610065, People's Republic of China

Southwest China; the event is known as the "6.17" Danba continuous disaster. Among these disasters, the debris flow and dammed lake lasted only approximately 1 day from the initiation to the end, but the outburst flood of the dammed lake triggered the reactivation of an ancient landslide on the left bank, resulting in the disruption of national highway G350 for approximately half a year. This is typical of sequential natural disasters with a strong amplification effect and long duration. The debris flows form as a result of the interaction of short-term intense rainfall and long-term accumulation of loose soils, gravels, rocks, and boulders in the tributaries. Once the accumulation of debris flows at the outlet reaches a certain level, the main river channel may be blocked, and a dammed lake is formed (Chen et al. 2005). The overtopping of dammed lakes is usually accompanied by dam failure and the formation of an outburst flood with a large flow (Jiang et al. 2018; Cai et al. 2020). The erosion caused by outburst floods during dam breakage can reduce the instability of riverbanks and riverbeds, leading to the occurrence of riverbank landslides or collapses.

To analyze the development process of this sequential disaster event, this paper focuses on the causes, processes, and mechanisms of debris flows, dammed lakes, and reactivated ancient landslides. Topographic and terrain data were collected by means of a three-dimensional terrestrial laser scanner (TLS), unmanned aerial vehicles (UAVs), and field surveys, and real-time kinematic (RTK) positioning was used for geo-registration (Gao et al. 2002). We independently analyze each disaster in the sequential disaster event and elaborate on their interactions. Based on on-site monitoring and quantitative deformation analyses, the motion process and reactivation mechanism of the ancient landslide are described.

The scale of this disaster event was tremendous, and its influences lasted for years, causing significant damage to the economy and security of Danba County. Therefore, we hope this study will provide valuable information for the follow-up management of these sequential disasters and insight into future similar hazards in Danba County, as well as useful information for studies of debris flows, dammed lakes, and reactivated landslides in other areas.

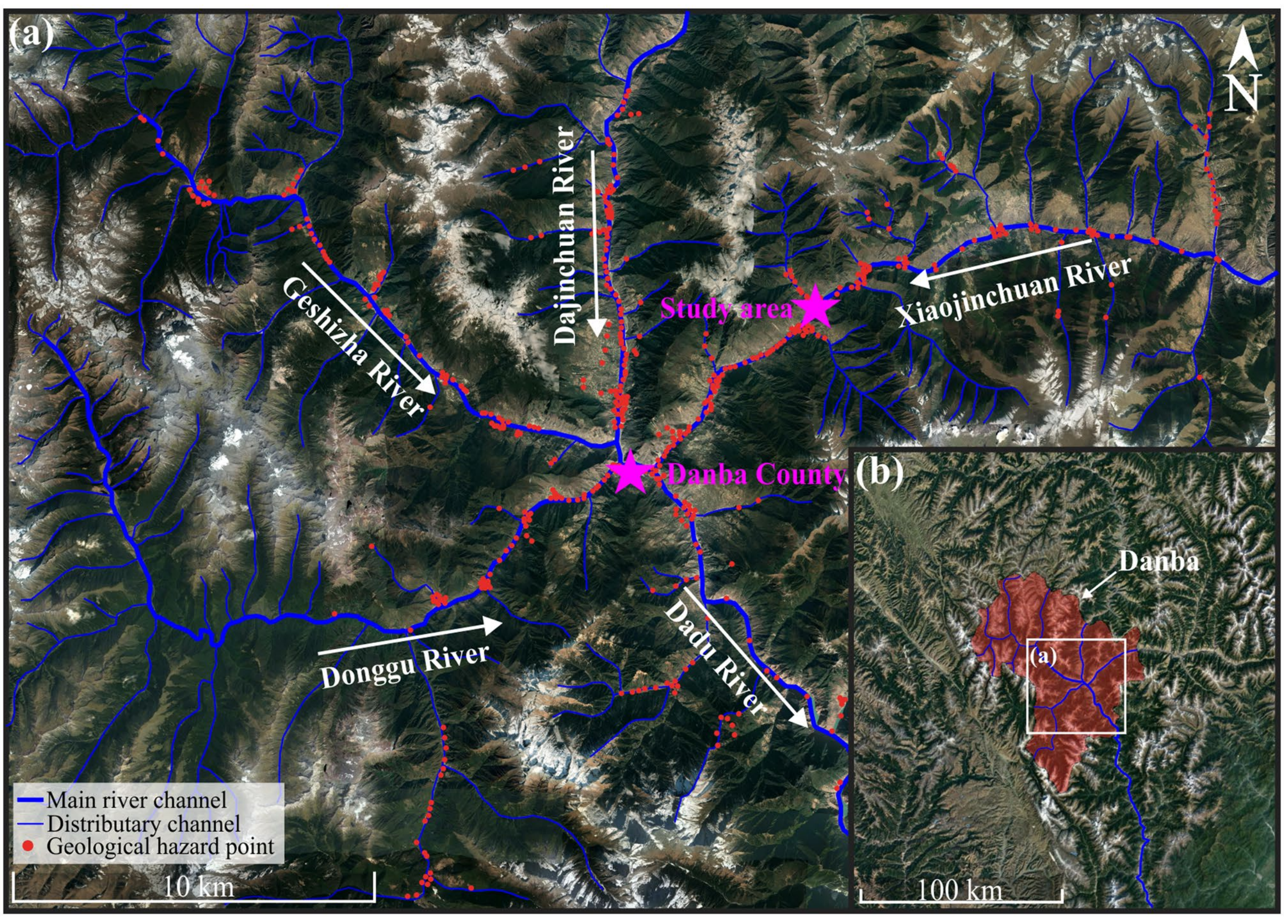

Fig. 1 Overall study area: (**a**) the distribution of the river channels and the statistics of geological disasters in Danba County and (**b**) the location of Danba County

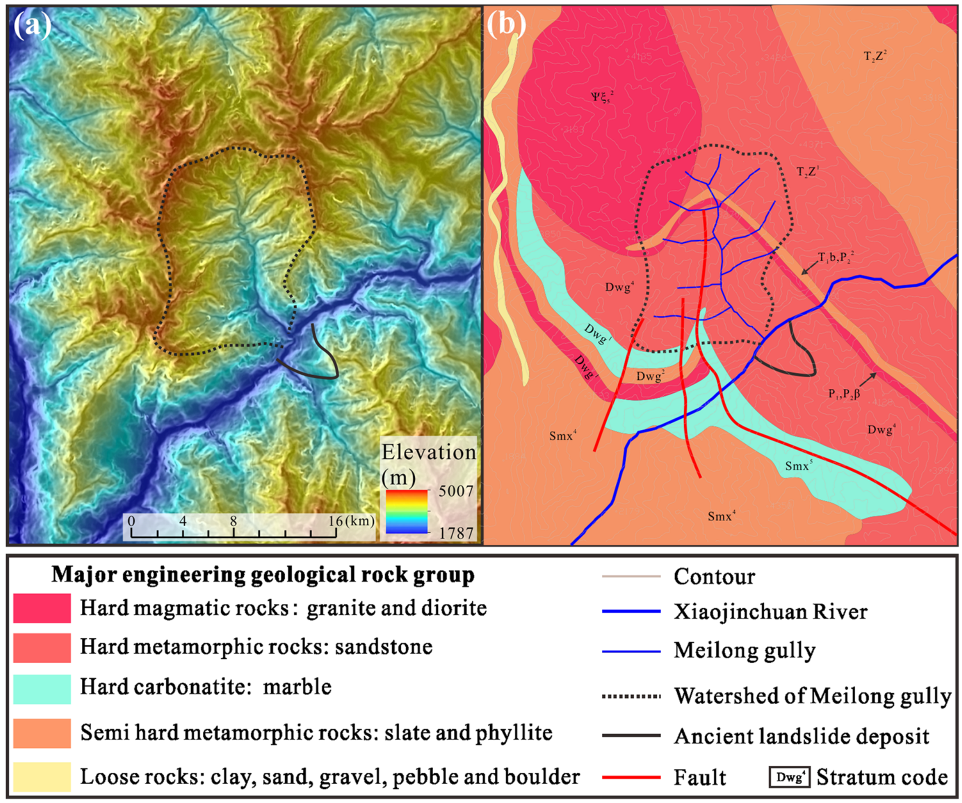

Fig. 2 Topography and geology of the study area: (**a**) topography of the study area and (**b**) engineering geology of the study area (Jiang et al. 2021)

Background and method

Study area

Danba County is located in the mountainous area of Southwest China (Fig. 1b), and its water system consists of five major rivers and hundreds of tributaries (Liu and Zhang 1994). Four main rivers, the Geshizha River (GSZ), Dajinchuan River (DJC), Xiaojinchuan River (XJC), and Donggu River (DG), converge in the middle of Danba County and flow into Dadu River (DD). Natural disasters in Danba County include debris flows, landslides, and collapses, which are mainly distributed along the five major rivers (Fig. 1a). The mid-high mountainous valley,

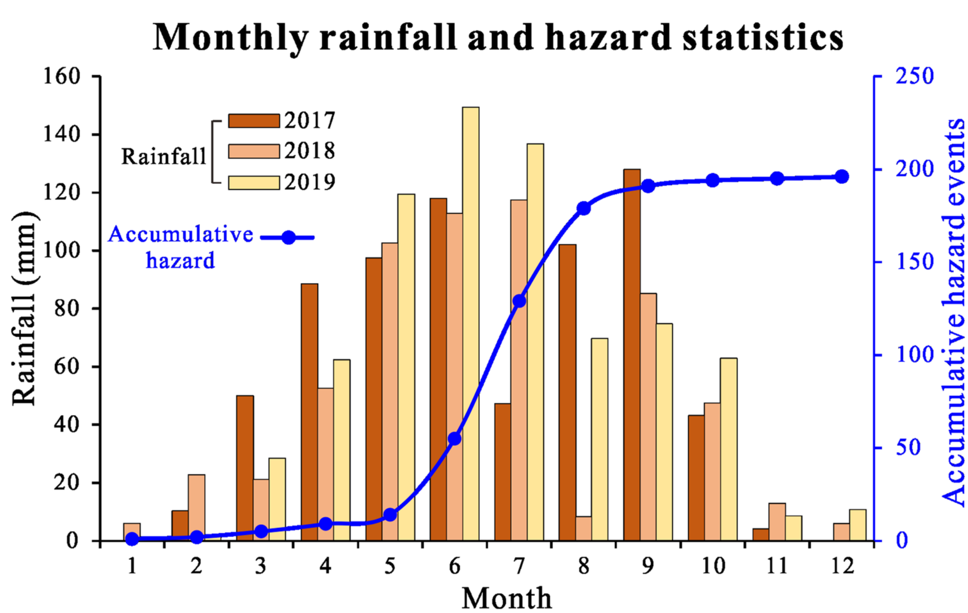

Fig. 3 Statistics of monthly rainfall and geological hazard events in the last 3 years

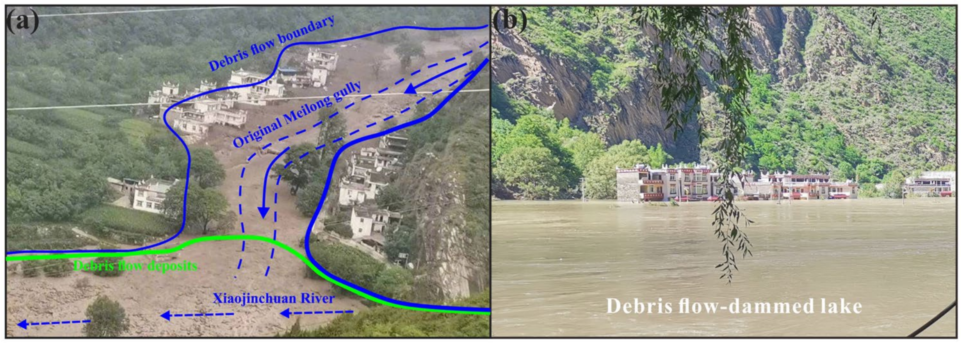

Fig. 4 Danba "6.17" sequential disaster event: (**a**) the 6.17 debris flow in Meilong gully, Danba County and (**b**) the debris flow-dammed lake upstream

vulnerable shallow ground surface, and heavy rainfall in the flood season are the main factors that led to the formation of these disasters (Zou et al. 2013).

The study area is located in the main stream of the XJC. The topography of the study area is an erosional and denudational alpine canyon. The elevations of the V-shaped valley range from 1787 to 5007 m (Fig. 2a). According to the major engineering geological rock grouping (Yu 2018), the stratigraphic lithology of the study area is part of the fourth rock group of the Wuiguan Group in Paleozoic Devonian (Dwg^4) strata. There are three reverse faults that cross part of the rainfall catchment area of the Meilong gully. The middle and shallow rock layers of the ancient landslide are mainly composed of black carbonaceous slate, gray marble, and quartzite, and the overburden is dominated by Quaternary avalanches and slope deposits (Fig. 2b).

According to a detailed investigation report of geological hazards in Danba County, debris flows account for approximately 40% of the annual natural hazards and mainly develop in Quaternary strata, including residual slope layers, avalanche layers, glacial flood layers, ancient debris flow deposit layers, and flood deposit layers. These layers vary in thickness and generally consist of loose soils or gravels. Landslides generally occur on slopes with angles of 25° to 40°. Multistage sliding accounts for most of the landslides, and the sliding surfaces are generally nearly parallel to the slope. Collapses usually occur on high and steep metamorphic rock strata with slope angles greater than 60°.

Rainfall is considered the key factor for the development of natural disasters in Danba County. Most of the tributary channels in Danba County are surrounded by high and steep mountains, leading to the concentration of surface runoff at the outlet of the rainfall collection area. According to the monthly rainfall statistics of the China Meteorological Administration and the natural hazard statistics of Danba County in the last 3 years (Fig. 3), rainfall-caused disasters account for 92% of the total disasters. Short periods of heavy rainfall in the summer bring an abundance of surface runoff for the formation of mountain torrents, debris flows, landslides, and collapses (Zhou et al. 2020a). In addition, glacial meltwater caused by high temperatures in the rainy season also increases the surface runoff discharge.

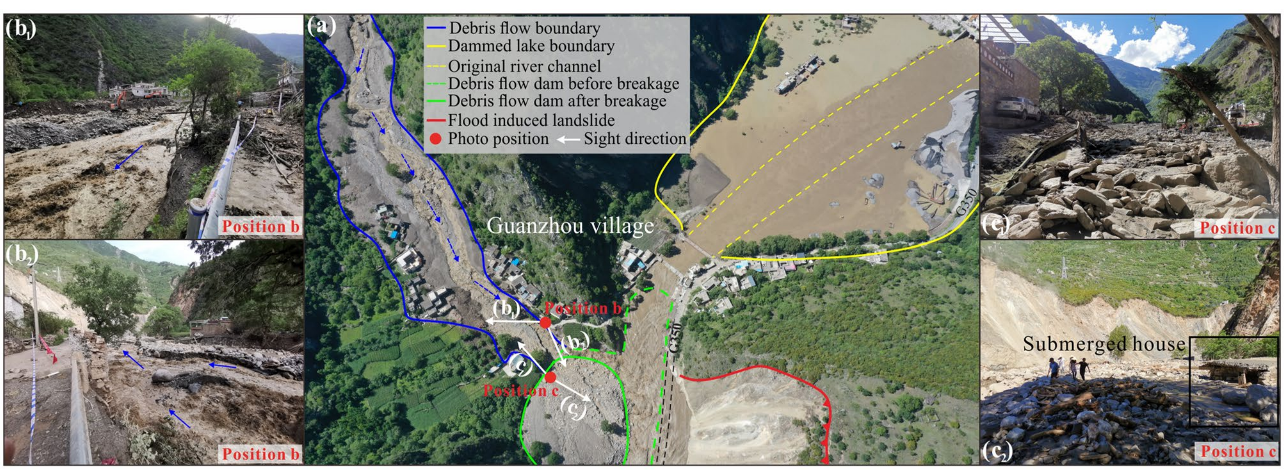

Fig. 5 Onsite investigation of the Danba 6.17 sequential disaster event: (**a**) overview of the debris flow deposits, landslide and dammed lake; (**b**$_1$)–(**b**$_2$) file images taken in position b; and (**c**$_1$)–(**c**$_2$) file images taken in position c

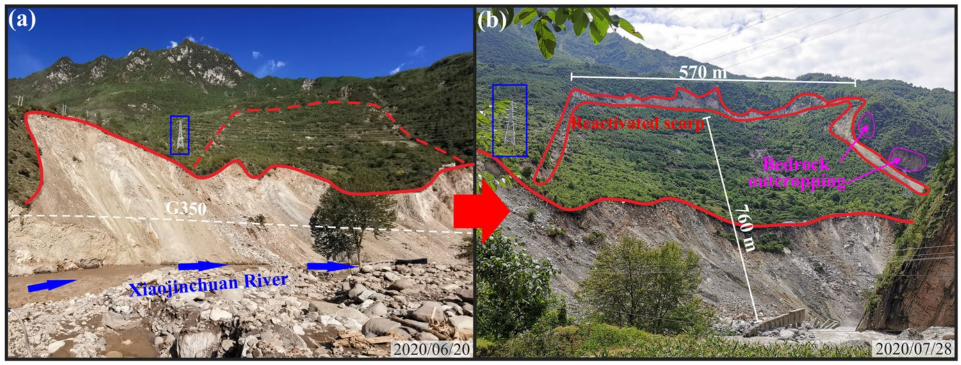

Fig. 6 Reactivation of the ancient landslide: (**a**) two days after the breakage of the debris flow dam and (**b**) one month after the breakage of the debris flow dam

The 6.17 Danba sequential disasters

At 3:20 a.m. on June 17, 2020, a large debris flow occurred in Meilong gully, Banshanmen town, Danba County (E102°01′32″, N30°58′57″). The debris flow, which was caused by a flash flood, brought large amounts of soils, fine sands, gravels, rocks, and boulders into the main channel of the XJC (Fig. 4a), thereby blocking the main river channel and leading to the formation of a dammed lake in the upstream Guanzhou Hydropower Station (Fig. 4b).

The total amount of material from the debris flow was approximately 848,000 cubic meters according to the disaster survey by the Water Conservancy Bureau of Danba County (WCBDC). The debris flow contained a large number of large rocks and boulders, which led to great losses in Guanzhou village (Fig. 5). Almost all the houses on the right

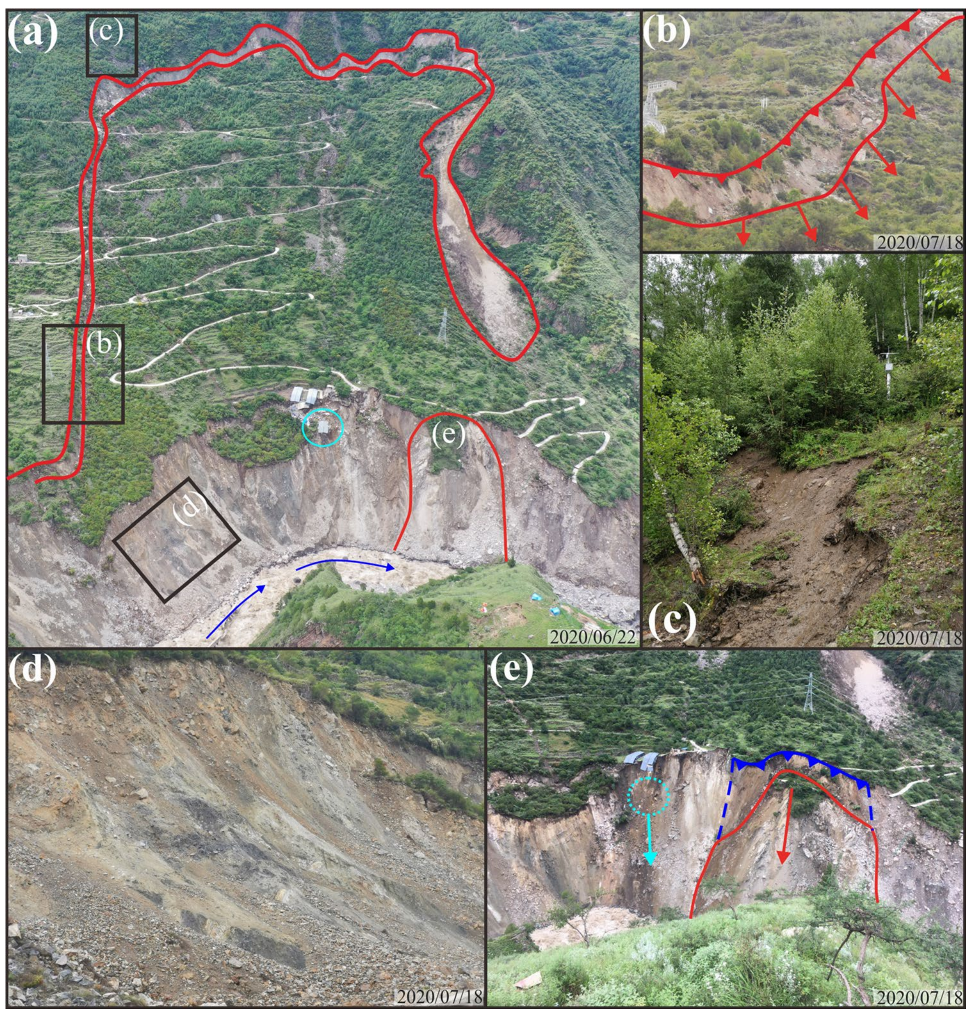

Fig. 7 Onsite investigation of the reactivated ancient landslide: (**a**) overview of the reactivated ancient landslide after 5 days; (**b**) lateral scarp of the reactivated ancient landslide; (**c**) new scarps appearing above the reactivated ancient landslide after one month; (**d**) image of the flood-induced landslide scarp; and (**e**) collapse and large-scale deformation of the flood-induced landslide scarp

bank of the Meilong gully were influenced by the debris flow, and casualties were reported (Fig. 5b_1 and b_2). The bridges and part of the roads were completely destroyed, and some houses near the outlet were submerged by the debris flow deposits (Fig. 5c_1 and c_2). According to the WCBDC, the water level reached the top of the debris flow dam at 4:00 p.m., which caused the overtopping of the debris flow dam. With the development of overtopping, the debris flow dam eventually failed, and the left bank slope was eroded by the dam break flood, resulting in the occurrence of landslides on the left bank and the destruction of national highway G350 (Fig. 6a). Large amounts of debris flow deposits and landslide masses were washed downstream, resulting in the uplift of the riverbed and the inundation of farmland, villages, and roads. In addition, the erosion of the left bank slope also led to the reactivation of an unstable slope: the Aniangzhai ancient landslide. These landslide deposits have existed for at least 100 years, according to a 72-year-old senior citizen in Guanzhou village. Within 1 month after the breakage of the debris flow dam, significant tensile cracks appeared along the back and lateral edges of the slope (Fig. 6b).

The earliest reactivation of the slope was concentrated in the river bend (Fig. 7a), and its main components were loose soils, gravels, and large stones with diameters of 0.5–2 m (Fig. 7d). With the deformation of the ancient landslide, the cracks along the back and lateral edge expanded over time (Fig. 7b), and new cracks in shallow layers began to appear on the top of the reactivated slope (Fig. 7c). Moreover, collapses, rockfalls, and subsidence occurred continuously on the flood-induced landslide scarp (Fig. 7e).

Data acquisition

To acquire the terrain information and monitor the development of the landslide, RTK, TLS, and UAVs were used in this study. TLS is a high-resolution remote sensing technique that rapidly acquires three-dimensional information of distant objects (Li et al. 2020; Jiang et al. 2020). Limited by the terrain, the TLS scan position can be set up only where people can physically reach, so it usually fails to obtain data in the presence of visual obstacles, which is especially obvious in mountain valleys (Li et al. 2019). In contrast, although the accuracy of UAV photogrammetry is lower than that of TLS, it has a faster speed and wider range in data acquisition (Dong et al. 2014; Koukouvelas et al. 2020a). Therefore, UAVs are suitable for large-scale topographic mapping, especially for the deformation monitoring of giant landslides. However, the accuracy of UAVs decreases rapidly in the absence of ground control points (GCPs), which are often difficult to set in landslide areas with limited access. In this paper, the reactivation of the

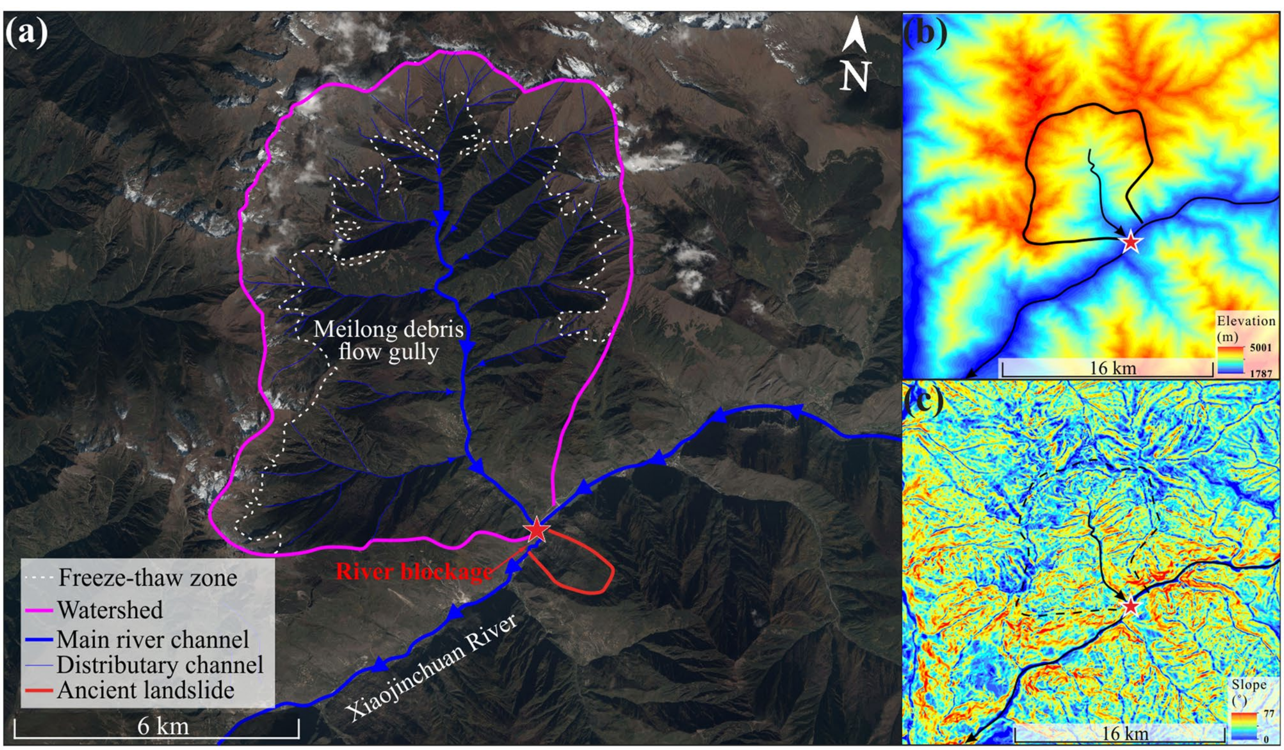

Fig. 8 Topography of the Meilong gully: (**a**) a satellite image of the Meilong gully (from Google Earth); (**b**) and (**c**) topography of Meilong gully

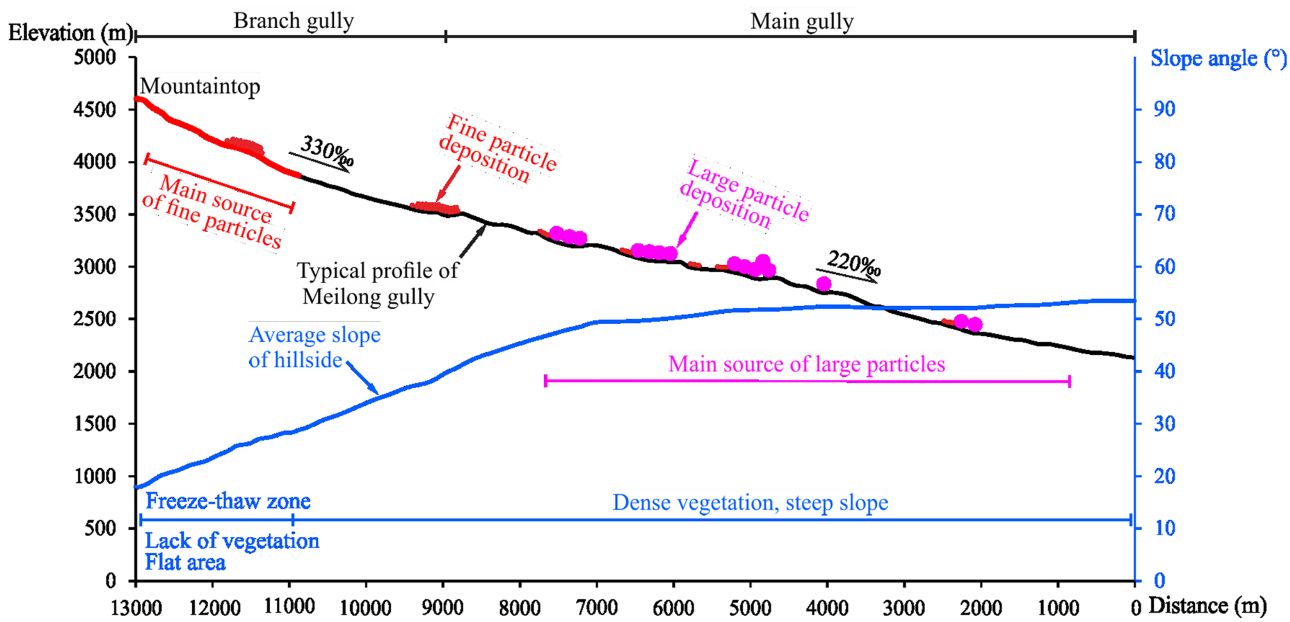

Fig. 9 Typical profile of the main Meilong gully

ancient landslide caused only the uphill road to be disrupted (Fig. 7a), so we could set up GCPs only within the river valley via RTK early in the disaster. In this case, we were faced with the dilemma that TLS cannot obtain a complete view of the entire landslide, and the accuracy of the UAV model and orthophoto decreases significantly with the distance from the RTK-based GCPs. To solve this problem, we extracted the spatial coordinates of obvious buildings, utility poles or boulders on the landslide surface from the high-precision TLS data and used them as the GCPs of the UAV. Furthermore, to verify the accuracy of this method, we conducted much research on the accuracy control and alignment methods of the point cloud data and finally realized the accurate alignment of UAV and TLS data in different periods (Jiang et al. 2021).

In this paper, we collected terrain data from 6 phases of TLS and 4 phases of UAVs. The TLS instrument was a RIEGL-VZ2000i, 3–5 scan positions were set in each phase of data collection, and the vertical and horizontal resolutions of TLS were set to 0.01°. The FeiMa-D2000, which was equipped with a Sony D-OP3000 camera, was used for UAV photogrammetry (FeiMa Robotics 2019). The aerial image resolution was 0.05 m, and the flight height was fixed at 300 m. Except for the RTK-based GCPs, we extracted 10 GPCs on the reactivated ancient landslide from the TLS data.

Results

Debris flow in the Meilong gully

The location of the Meilong debris flow is approximately 19.5 km upstream of Danba County. The rain collection range is surrounded by steep mountains on all sides and has an area of 64.37 km^2 and a maximum height of 2500 m (Fig. 8). The minimum width of its outlet is only 113 m. There are freeze–thaw areas at the top of the mountain (from elevation (EL.) 4000 m to EL. 5000 m), with average slopes between 0° and 30° (Fig. 8c). The slopes below the freeze–thaw areas are relatively steep (30°–60°) with elevations between 2300 and 4000 m.

Table 1 Statistics and classification of debris flows in Danba County

Scale	Slope of hillside (°)			Gradient of gully (‰)		
	< 25	25–40	> 40	< 250	250–400	> 400
Giant	1	0	4	3	1	1
Large	0	4	19	11	11	1
Medium	0	12	32	14	15	15
Small	2	9	29	7	19	14

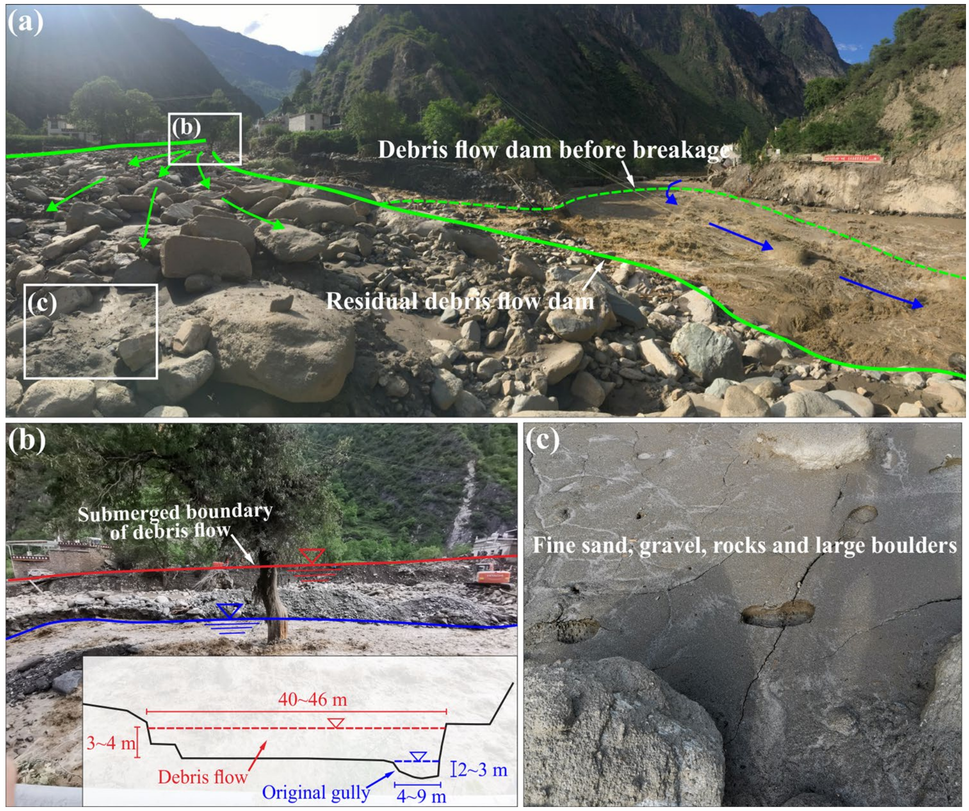

Fig. 10 Onsite investigation of the debris flow deposits: (**a**) debris flow deposits; (**b**) submerged area of the debris flow; and (**c**) major components of the debris flow deposit

Figure 9 shows a typical profile of the Meilong gully and the average slope angle of the nearby hillside. The surface overburden in the freeze–thaw areas is a Quaternary deposit layer with abundant fine particles. According to a geological hazard report in 2006, the statistical relationship between the scale of the debris flow, slope of the hillside, and gradient of debris flow gullies in Danba County is shown in Table 1. This shows that giant debris flows were more likely to occur in gullies with gradients less than 240‰ and hillside slopes greater than 40°, which is consistent with the characteristics of the Meilong gully.

According to the on-site investigation of the residual debris flow deposits (Fig. 10a), the main components of the debris flow are soils, fine sands, rocks, and boulders, and the particle size distribution ranges from less than 1 mm to more than 5 m (Fig. 10c). We counted the stones exposed on the debris flow deposits near Guanzhou village and found that almost all the rocks with a diameter of more than 0.5 m have experienced strong weathering and erosion, indicating that they have resided within the Meilong gully for a long time and have been eroded by water flow throughout the year. We described a typical cross-section of the Meilong gully to show its shape after the 6.17 debris flow (Fig. 10b) according to the submerged area in Guanzhou village. Then, we depicted several cross-sections based on TLS data and flood traces in the flooded area and simplified the real section into a trapezoidal section with a slope angle of 45°. According to Manning's formula (Attari and Hosseini 2019; Tuozzolo et al. 2019), the discharge of the debris flow in the Meilong gully is calculated in Table 2. The formula is

$$V = \frac{1}{n} \times R^{\frac{2}{3}} \times i^{\frac{1}{2}} \quad (1)$$

where n is the roughness coefficient of the gully, R is the hydraulic radius, and i is the gradient of the gully.

The results show that the flood discharge of the Danba 6.17 debris flow was approximately ten times the normal discharge.

Table 2 Discharge estimation for the Meilong gully, where n is the roughness coefficient of the gully; b_1 and b_2 are the average bottom and top widths of the cross-section, respectively; i is the gradient of the Meilong gully; h is the average water depth; v is the average velocity of the cross-section; and Q is the discharge of the Meilong gully

Parameter	n	b_1 (m)	b_2 (m)	i (‰)	h (m)	v (m/s)	Q (m^3/s)
Normal	0.04	4 (±0.5)	9 (±0.5)	220	2.5 (±0.5)	2.2 (±0.1)	35 (±5)
Flood	0.04	35 (±0.5)	41 (±0.5)	220	3.5 (±0.5)	3.3 (±0.1)	412 (±47)

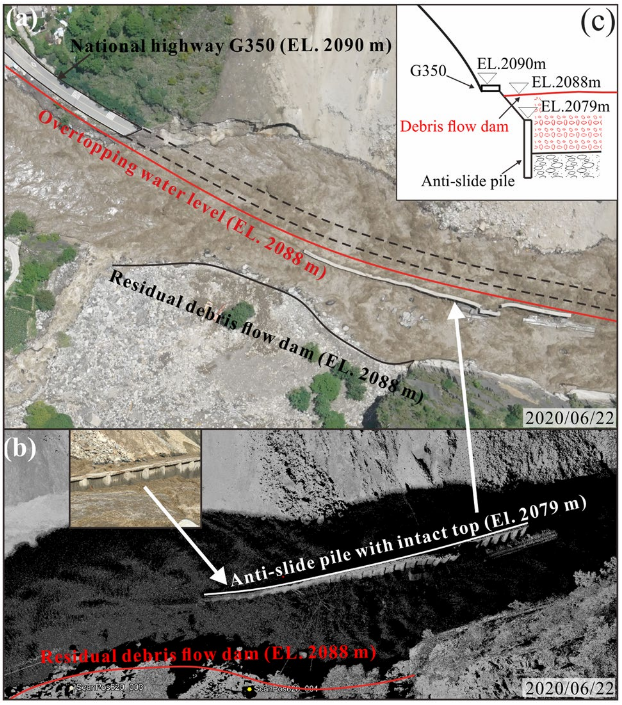

Fig. 11 On-site investigation and TLS data of the ground features: (**a**) overview of the investigated ground features; (**b**) TLS data for extracting the elevation of ground features; and (**c**) typical profile for the analysis of debris flow dams

Dynamic evolution of the debris flow-dammed lake

The time interval between the formation and destruction of the debris flow dam was only a few hours. Therefore, it is very difficult to obtain actual image or terrain information on the dam formation and failure processes in subsequent studies. To reproduce the dynamic evolution of the debris flow dam, we carefully analyzed the TLS data on Jun. 20, 2020 and conducted a detailed field survey in an attempt to infer the formation and destruction of debris flow dams using some typical ground features.

Because of the existence of the ancient landslide, anti-slide piles were used as the foundation of national highway G350. Some of the anti-slide piles were destroyed in the flood-induced landslide, while others were preserved (Fig. 11a). As shown in Fig. 11b, most of the top beams of the preserved anti-slide piles were intact. According to the TLS data, we extracted the elevations of G350 (EL. 2090 m), the top of the anti-slide pile (EL. 2079 m), and the edge of the residual debris flow dam (EL. 2088 m) and then restored a typical section of the river channel before dam breakage (Fig. 11c).

According to the elevation of these ground features, we speculate on the development of the breakage of the debris flow dam and the flood-induced landslide on the left bank. At first, the debris flow brought particles of various sizes into the main channel of the XJC and blocked the river channel (Fig. 12a). The anti-slide pile was completely buried by debris flow deposits (Fig. 12b). Generally, debris flow deposition is fan-shaped, and the height of the front edge is relatively low (Chen et al. 2013; Hu et al. 2019; Wang et al. 2017). Therefore, the initial overtopping might have occurred near the intersection of debris flow deposits and the left bank slope (Fig. 12b). As erosion developed at the slope toe, the bank slope gradually lost its stability. Two types of landslide surfaces might exist in this situation: (a) the sliding surface of the landslide is deep, and the anti-slide pile is damaged by the direct impact of the landslide (Fig. 12c_1 and d_1); (b) the sliding surface was shallow, and the landslide occurred above the anti-slide pile, resulting in the anti-slide pile remaining intact (Fig. 12c_2 and d_2). Then, because of the existence of the dammed lake and the increased upstream flow in the flood season, the water level at the breach was much higher than usual, which had a strong erosion effect on the left bank landslide residues, resulting in the continuous occurrence of landslides, collapses, subsidence, and rockfalls.

Monitoring of the ancient landslide

According to the monitoring results, the ancient landslide can be divided into two stages and five zones (Fig. 13a). The reactivation of the lower stage (Stage I) began with the dam break flood, which can be subdivided into four smaller zones (zones I, II, III, and IV) according to the accumulated deformation. Zone I is the scarp of the flood-induced landslide, with a length of approximately 650 m along the river and an average width of approximately 180 m along the slope. The height of this area is approximately 70 m, and the slope is approximately 40 degrees. Zone II is the area with the largest deformation during the landslide, which can be divided into two parts: Zone II_1 and Zone II_2. Zone II_1 is the main landslide mass and Zone II_2 is the reactivated scarp of Zone II_1, as well as the toe of Zone V (stage II). Zone III is the upstream triangular-shaped area whose deformation process is controlled by the instability of its toe and the lateral restraint in Zone II_1. The length along the slope is approximately 700 m, and the top and bottom widths are approximately 300 m and 100 m, respectively. Zone IV is a downstream syncline bedrock on which two bedrock outcrops appeared. There is no significant displacement in this area. The reactivation of Zone V (stage II) is approximately 1 month later than that of stage I, with a small sliding distance and good integrity. There are obvious tension cracks on its trailing edge, ranging in width from 4 to 10 m (Fig. 13b and c). In addition, there was a significant horizontal displacement of the anti-slip pile on the riverbed, which moved approximately 15 m toward the opposite bank a few months after reactivation (Fig. 13d and e).

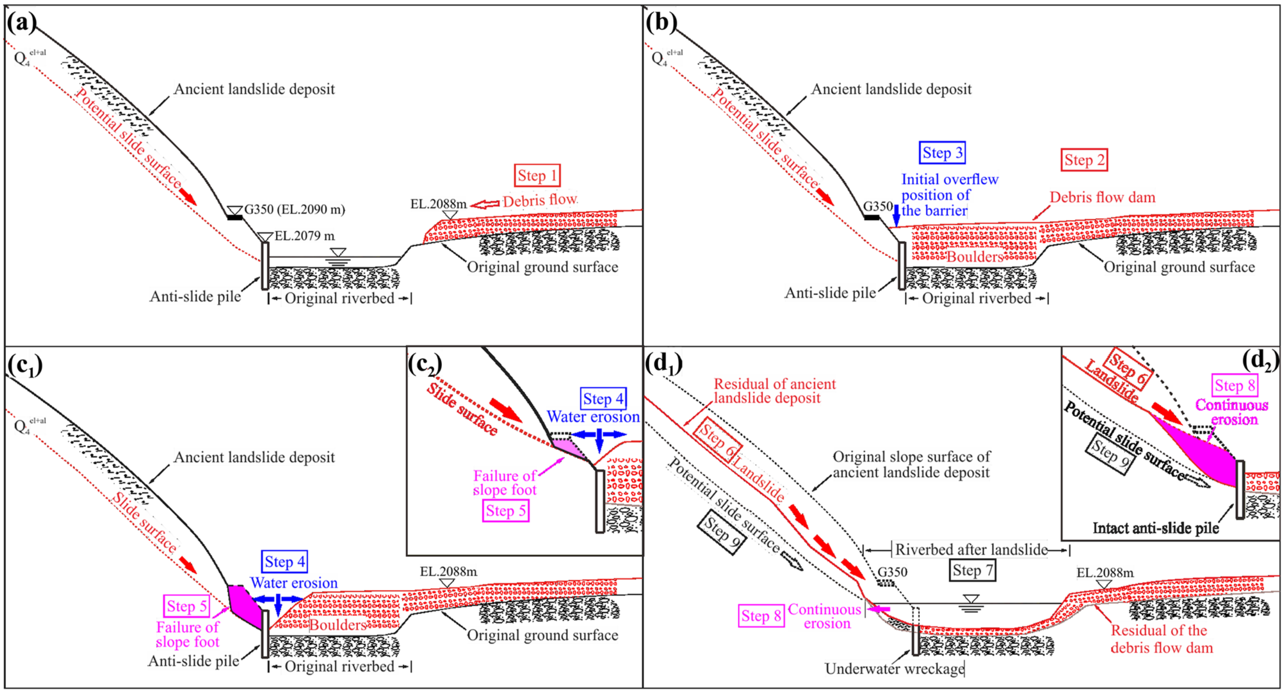

Fig. 12 Formation and breakage of the debris flow dam: (**a**) typical profile of the original river channel; (**b**) river blockage by the debris flow dam; (**c$_1$**) and (**c$_2$**) overtopping of the debris flow dam and the erosion process of the water; and (**d$_1$**) and (**d$_2$**) process of the flood-induced landslide

Based on the above observations, we first used the 3D point cloud generated by UAV aerial photography to quantitatively analyze the overall deformation of the landslide. Figure 14 shows the deformation of the landslide in the first month (Fig. 14a) and in the second to third months (Fig. 14b). As a result, the accumulated deformation and failure mode of the ancient landslide varied spatially and temporally. The most obvious phenomenon is that the overall

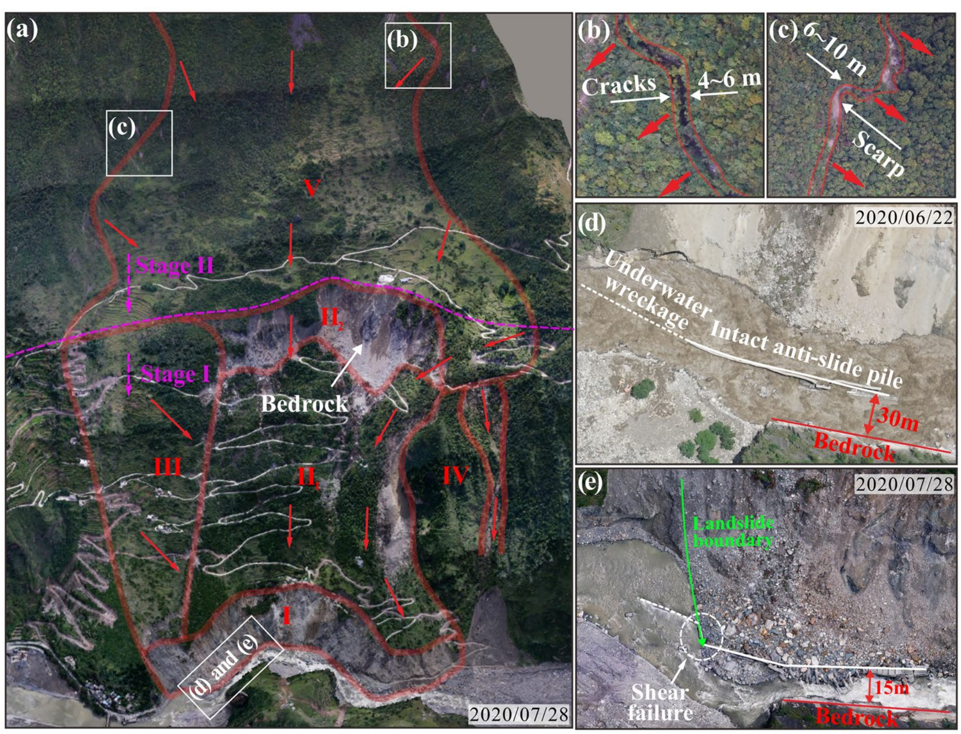

Fig. 13 Deformation of the reactivated ancient landslide after one month: (**a**) overview of the ancient landslide; (**b**), (**c**) cracks and scarps at the back edge of the ancient landslide; and (**d**), (**e**) horizontal displacement of the slope toe from 2020 Jun 22 to 2020 Jul 28

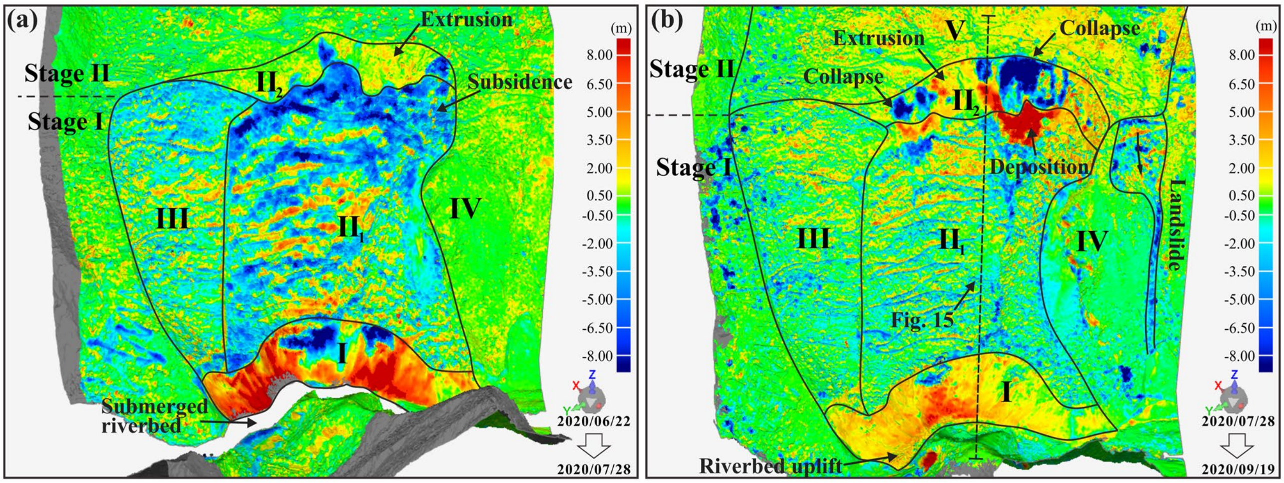

Fig. 14 3D deformation analysis based on point cloud data obtained from UAV photogrammetry: (**a**) 3D deformation from 2020 Jun 20 to 2020 Jul 28 and (**b**) 3D deformation from 2020 Jul 28 to 2020 Aug 19

deformation of the landslide gradually decreases, but the deformation area expands significantly. During the first month, the deformation area was mainly concentrated in stage I, and the maximum deformation appeared in Zone II_1. The slope mass in this area slid down along the slope, which led to the extrusion, collapse, and subsidence of the slope toe (Zone I). In the next 2 months, the deformation of stage I slowed down to a large extent, while stage II started to show a significant displacement. Stage II gradually destabilized after losing the restraint from Zone II_1, and its slope toe exhibited obvious outward extrusion and collapse.

Figure 15a shows a typical profile of the 3D deformation map in Fig. 14b. The deformation mode of zone I can be deduced by Fig. 15c:

1. Subsidence on the back edge

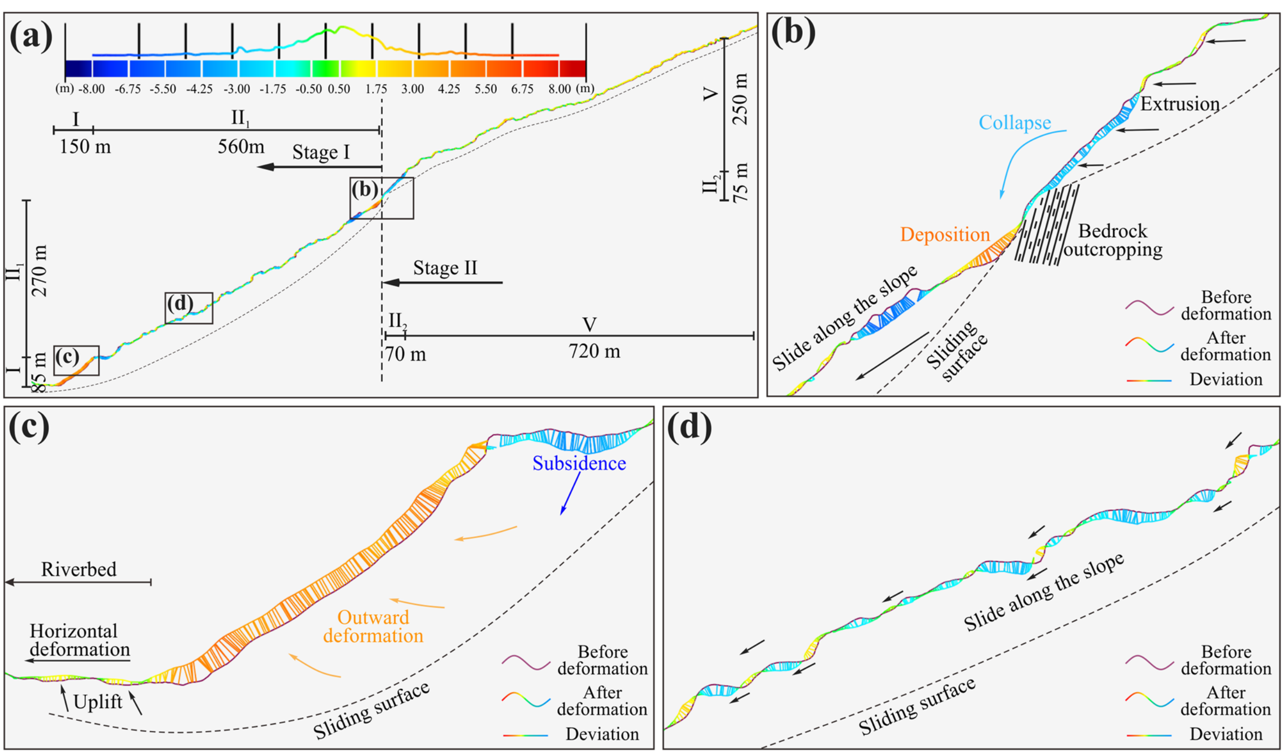

Fig. 15 Typical profile of the 3D deformation map: (**a**) overall profile and (**b**)-(**d**) local deformation diagram in Zones II_2, I and II_1

2. Outward extrusion and uplift on the front edge
3. Uplift and horizontal displacement of the riverbed

The most obvious difference between the deformation forms of Zones I and II_2 is the rotation deformation at the front edge (Fig. 15c). Although the cause of the reactivation of both stages I and II was the instability of the front edge, the former underwent a rotational deformation in which the front edge lifted and the trailing edge subsided. As a result, the sliding surface of stage I should be located below the riverbed, which is the only way to cause the uplift and horizontal displacement of the riverbed.

The shortest distance (SD) method is used to measure the 3D deformation based on point cloud data. The method selects the points closest to the reference point set from the test point cloud set and considers the distance between the points as the amount of deformation. In this method, the deformation nephograms in Zones II and III are distributed in red and blue stripes. This is because the surfaces of the slope before and after the deformation crisscross each other, and the tie points selected by the SD method were not the real points before and after the deformation (Fig. 15d). Therefore, to compensate for the defects of the SD method, we use the difference in orthophotos (DOO) to analyze the sliding process of the landslide mass along the slope (Fig. 16). The displacement identified from the DOO can be analyzed based on manual visualization or offset pixel tracking, such as Cosi-Corr (Ayoub et al. 2009). Since the relative deformation of the ground surface is clearly visible and regular, we manually extract the characteristic points of the ground surface before and after deformation in the UAV images, such as roads, houses, utility poles, and vegetation, to analyze the landslide displacement.

As a result, the use of the DOO allows a better visualization of the ancient landslide sliding down the slope. Since the maximum slope angle of the ancient landslide is less than 45° (approximately 40°), there is a certain degree of synchronization between the horizontal displacement and the actual displacement, and the horizontal displacement can reflect the actual displacement to a certain extent. In addition, this method can overcome the data shortage caused by the lack of point cloud data. For example, due to the high

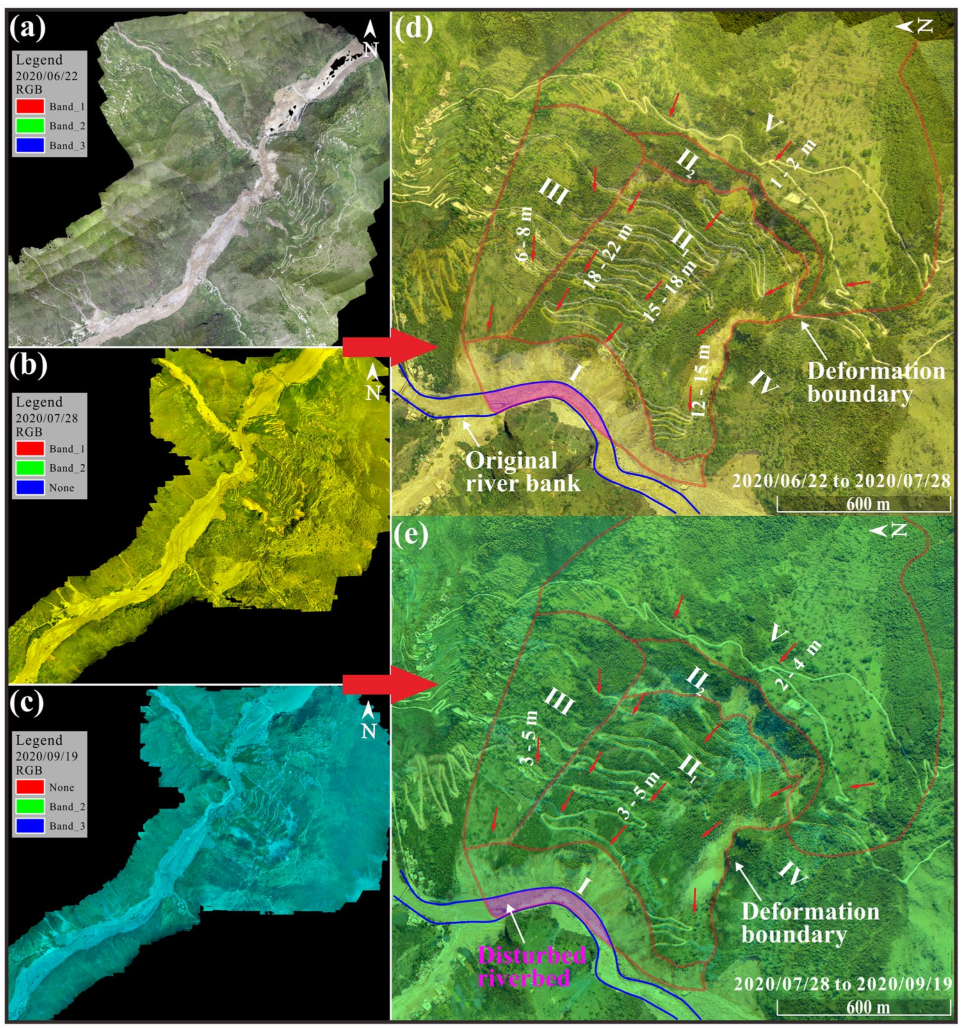

Fig. 16 Horizontal displacement based on the differences in orthophotos (DOO): (**a**)-(**c**) UAV orthophotographs on 2020 Jun 20, 2020 Jul 28, and 2020 Aug 19 in different color bands and (**d**), (**e**) horizontal displacement of the ancient landslide

water level in the first month, it is difficult to obtain the terrain of the riverbed (Fig. 14a), so it is difficult to analyze the evolution of the riverbed in the first month by means of 3D analysis. Instead, we determined the boundary of the landslide by means of the DOO and found that part of the riverbed deformed synchronously with the ancient landslide. Moreover, we quantitatively analyzed the horizontal displacement of the ancient landslide and found that the cumulative horizontal displacements in Zone II and Zone III were 12–22 m and 6–8 m, respectively, in the first month, and the maximum displacement occurred at the junction of Zone II and Zone III (approximately 18–22 m).

Reactivation of the ancient landslide

There are two possible factors causing the instability of the ancient landslide: one is the lateral erosion of the outburst flood, which causes the instability of the left bank slope and the reduction of the anti-slide force; the other is the vertical erosion, which causes the undercutting of the riverbed and the reduction of the anti-slide force. In the first case, there is a high probability that the exit of the sliding surface will appear above the riverbed, while in the second case, the exit of the sliding surface may appear below the riverbed.

Based on the boundary of the DOO and the original riverbank, we determined the boundary of the disturbed riverbed and the exit of the sliding surface. Then, the horizontal displacement of the riverbed was determined by quantitatively calculating the horizontal displacement of the anti-slide piles and the large boulders in the riverbed (Fig. 17a). From these results, we drew three typical profiles of the disturbed riverbed (Fig. 17b–d). The maximum width of the disturbed riverbed appeared on the upstream side (profile A-A′), and the horizontal displacement of the riverbed was approximately 20–23 m, which was almost equal to the horizontal displacement of the ancient landslide above this area in Fig. 16d (18–22 m in the first month and 3–5 m in the next 2 months). Similarly, the horizontal displacement of profile B-B′ was almost the same as that of the upper ancient landslide. It can be determined that this part of the disturbed riverbed deformed synchronously with the ancient landslide, indicating that the exit of the sliding surface of the ancient landslide had penetrated into the river channel. In contrast, the DOO boundary in profile C–C′ was on the slope surface of Zone I, and the riverbed in this area was stable.

It can be inferred that the reactivation of the ancient landslide was related to both slope erosion and riverbed undercutting. The undercutting of the riverbed caused deep sliding of the ancient landslide, resulting in synchronous deformation of the riverbed and the ancient landslide, while slope erosion caused shallow sliding of the slope. The main reasons for the different deformation modes of the three profiles include the deposition range of the debris flow dam, the shape of the river channel, and the topographic constraints. Profile C–C′ was located downstream of the ancient landslide, which was far from the debris flow dam, so the erosion effect of the dam break flood was the weakest. Compared with profile B-B′, profile A-A′

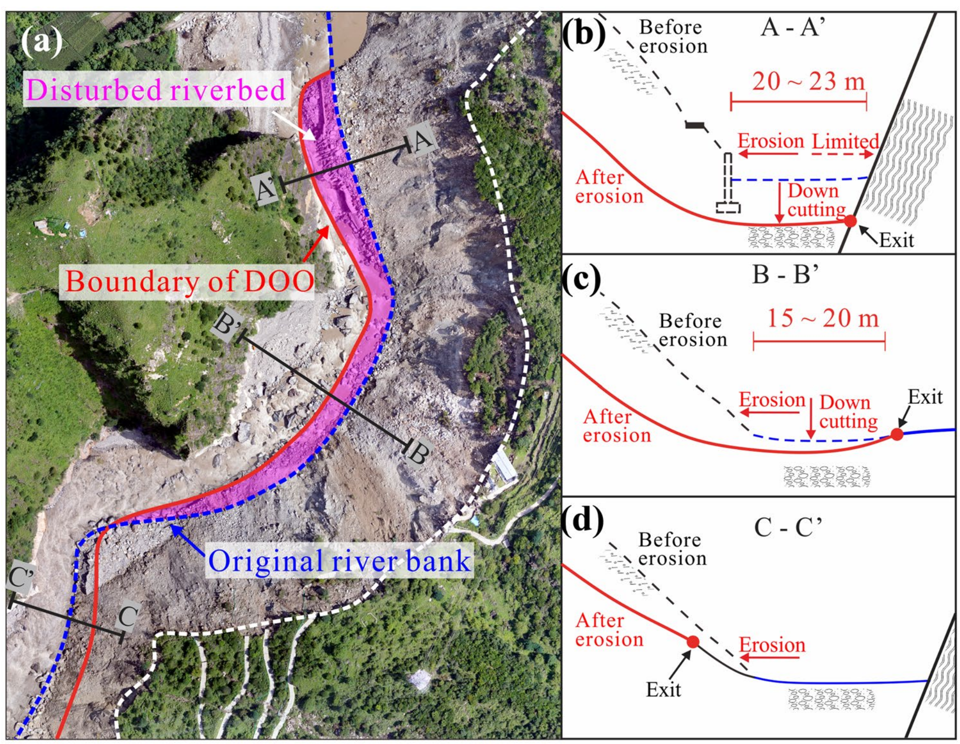

Fig. 17 Analysis of the landslide boundary: (**a**) determination of the range of the disturbed riverbed based on the DOO; (**b**)–(**d**) typical profiles of the riverbed

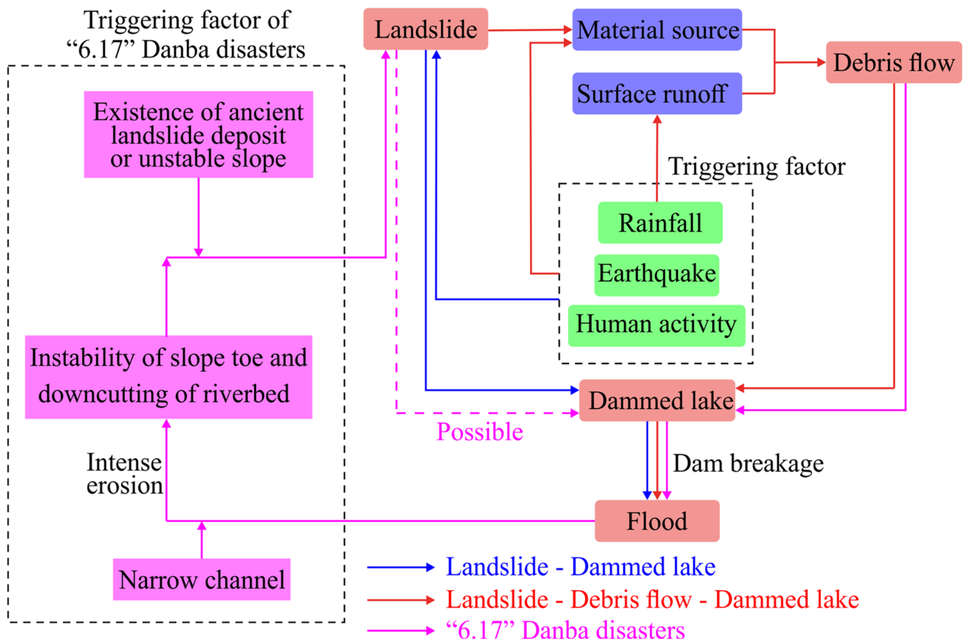

Fig. 18 Schematic diagram of the mechanism of continuous disasters: landslide-dammed lake disasters (blue lines), landslide-debris flow-dammed lake disasters (red lines) and the 6.17 Danba disasters (purple lines)

was closer to the debris flow dam. Moreover, the narrow channel and hard bedrock on the opposite bank limited the expansion of the spillway during the outburst flood, leading to increased vertical erosion and more severe disturbance of the riverbed. Therefore, the riverbed disturbance in profile A-A′ was larger, which was reflected in the larger horizontal displacement in this section.

Discussions

Debris flows, landslides, collapses, and dammed lakes are common disasters in mountainous areas. The occurrence of one of these disasters usually results in a succession of the other disasters, thereby forming sequential disaster events. The form of the Danba 6.17 sequential disaster event is a

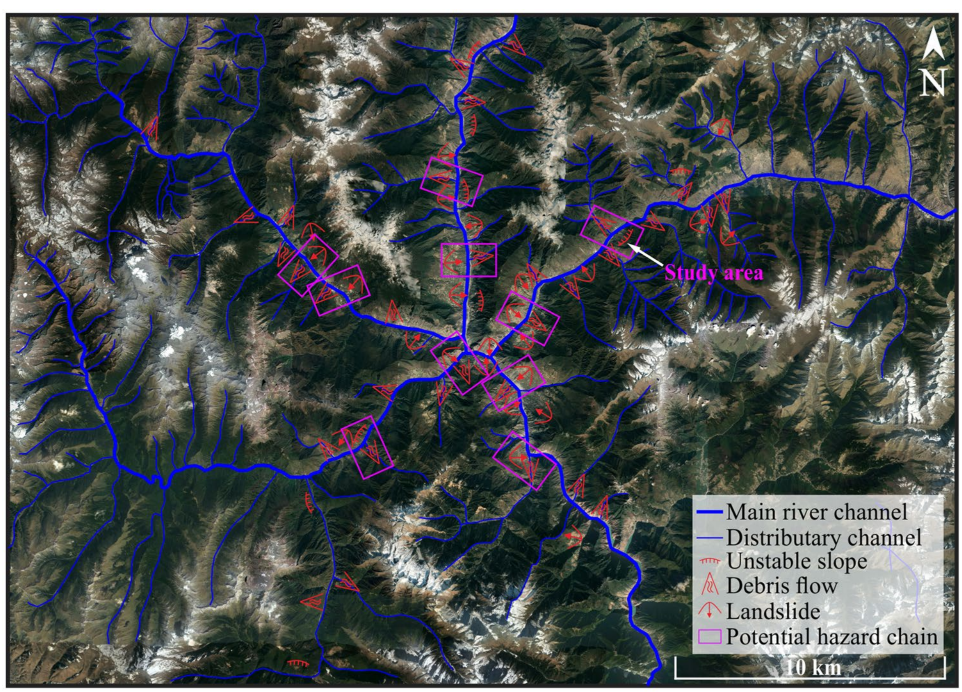

Fig. 19 Potential sites similar to the 6.17 Danba sequential disasters in Danba County

debris flow–dammed lake-reactivated landslide, which has a longer duration and greater potential risk than a normal dammed lake disaster (Fig. 18). The key factor in the formation of this type of sequential disaster event is the presence of an ancient landslide or unstable slope at the site of the debris flow dam. Dam failure floods may cause the instability of unstable slopes and have the potential to block river channels. According to geological surveys, there are dozens of ancient landslides or unstable slopes in Danba County. To determine whether other sequential disaster events similar to the Danba 6.17 sequential disasters could occur in these areas, we counted the locations of existing natural hazards, including debris flows, landslides, and unstable slopes, according to the detailed investigation report of geological hazards in Danba County (Fig. 19). Nine positions with ancient landslides or unstable slopes located at the outlet of debris flow gullies were highlighted. All of the positions are located near the main river channel, and the formation of a large debris flow may form such continuous disasters, seriously affecting regional safety and economic development in downstream areas.

The reactivation of ancient landslides induced by dam break floods greatly promoted the potential severity and prolonged the duration of the disasters. During the breakage of the debris flow dam, the lateral erosion of the outburst flood caused slope instability and the formation of lateral free surfaces, while vertical erosion caused riverbed disturbance and a reduction in the shear strength of the slope toe. With further deformation of the ancient landslide toward the opposite bank, the disturbed riverbed was gradually compacted, and the shear strength of the slope toe increased, leading to the weakening of the deformation rate of the ancient landslide. In the flood season, the lateral erosion of water flow is unlikely to cause deep destabilization of the riverbed, but shallow collapses or landslides may still occur in zone I. If the landslide is large enough, narrow channels (e.g., the A-A′ profile) may be blocked again. Even if the volume of the barrier is small, the outburst flood may again adversely affect the stability of the deeper part of the riverbed and lead to the reactivation of the ancient landslide again.

Conclusions

The main components of the Danba 6.17 sequential disasters include the large-scale debris flow, the subsequent debris flow-dammed lake, and the reactivation of an ancient landslide after dam failure. The discharge of the debris flow was approximately ten times that of the normal flow. The long-term accumulation of a large number of solids in the Meilong gully and the flash flood triggered by short-term heavy rainfall were the main causes of the debris flow. The breakage of the debris flow dam induced an outburst flood that intensely eroded the riverbed and the slope toe of the left bank, leading to the reactivation of the ancient landslide.

On-site monitoring and quantitative deformation analyses were conducted based on TLS and UAVs. The reactivated ancient landslide was a two-stage landslide, and the upper part was reactivated approximately 1 month later than the lower part. The main deformation modes of the landslide include the main body sliding along the slope and the rotational deformation at the front edge. The landslide was deformed to a greater extent during the first month, while the deformation rapidly decreased in the next 2 months. Based on the differences in orthophotos, the extent and horizontal displacement of the disturbed riverbed were determined, and the depth of the sliding surface of the landslide on the upstream side was found to be greater than that on the downstream side. As a result, the undercutting of the riverbed could cause the deep sliding of the ancient landslide, while lateral erosion could lead to shallow sliding at the slope toe.

Acknowledgements Critical comments by the anonymous reviewers greatly improved the initial manuscript.

Funding We received support from the National Natural Science Foundation of China (41977229 and U20A20111), the National Key R&D Program of China (2017YFC1501102), and the Sichuan Youth Science and Technology Innovation Research Team Project (2020JDTD0006).

References

Attari M, Hosseini SM (2019) A simple innovative method for calibration of Manning's roughness coefficient in rivers using a similarity concept. J Hydrol 75810–823. https://doi.org/10.1016/j.jhydrol.2019.05.083

Ayoub F, Leprince S, Avouac JP (2009) Co-registration and correlation of aerial photographs for ground deformation measurements. ISPRS J Photogramm Remote Sens 64(6):551–560

Brideau MA, Shugar DH, Bevington A, Willis M, Wong C (2019) Evolution of the 2014 Vulcan Creek landslide-dammed lake Yukon Canada using field and remote survey techniques. Landslides 16:1823–1840

Cai YJ, Cheng HY, Wu SF, Yang QG, Wang L, Luan YS, Chen ZY (2020) Breaches of the Baige Dammed lake: Emergency response and dam breach flood. Sci China Technol Sci 63(7):1164–1176

Cui P, Xiang LZ, Zou Q (2013) Risk assessment of highways affected by debris flows in Wenchuan earthquake area. J Mt Sci 10(2):173–189

Chen N, Li T, Gao Y (2005) A great disastrous debris flow on 11 July 2003 in Shuikazi valley Danba County western Sichuan China. Landslides 2:71–74

Chen GQ, Li YG, Zhang YB, Wu J (2013) The disaster chain of earthquake induced landslides. In: Ugai K, Yagi H, Wakai A (eds) Earthquake-Induced Landslides. Springer, Berlin Heidelberg, pp 949–958

Chen KT, Chen XQ, Niu ZP, Guo XJ (2019) Early identification of river blocking induced by tributary debris flow based on dimensionless volume index. Landslides 16:2335–2352

Dong JJ, Lai PJ, Chang CP, Yang SH, Yeh KC, Liao JJ, Pan YW (2014) Deriving landslide dam geometry from remote sensing images for

the rapid assessment of critical param related to dam-breach hazards. Landslides 11:93–105
FeiMa Robotics (2019) http://www.feimarobotics.com/zhcn/productDetailD2000. Accessed 28 Jun 2019
Gao Y, Liu Z, Liu Z (2002) Internet-based real-time kinematic positioning. GPS Solut 5:61–69
Ge YG, Zou Q, Zhang JQ, Guo XJ (2017) Characteristics causes and hazards of large-scale debris flows on June 23 at Haitong Watershed Tibet China. In: Mikoš M, Casagli N, Yin Y, Sassa K (eds) Advancing Culture of Living with Landslides. Springer, Cham, pp 581–592
Hu GS, Zhao CY, Chen NS, Chen KT, Wang T (2019) Characteristics mechanisms and prevention modes of debris flows in an arid seismically active region along the Sichuan-Tibet railway route, China: a case study of the Basu-Ranwu section southeastern Tibet. Environ Earth Sci 78:564
Hu T, Huang RQ (2017) A catastrophic debris flow in the Wenchuan Earthquake area July 2013: characteristics formation and risk reduction. J Mt Sci 14(1):15–30
Jiang N, Li HB, Hu YX, Zhang JY, Dai W, Li CJ, Zhou JW (2021) A monitoring method integrating terrestrial laser scanning and unmanned aerial vehicles for different landslide deformation patterns. IEEE J Sel Top Appl Earth Obs Remote Sens 14:10242–10255
Jiang N, Li HB, Liu MS, Zhang JY, Zhou JW (2020) Quantitative hazard assessment of rockfall and optimization strategy for protection systems of the Huashiya cliff southwest China. Geomatics Nat Hazards Risk 11:1939–1965
Jiang XG, Huang JH, Wei YW, Niu ZP, Chen FH, Zou ZY, Zhu ZY (2018) The influence of materials on the breaching process of natural dams. Landslides 15:243–255
Koukouvelas IK, Nikolakopoulos K, Zygouri V, Kyriou A (2020a) Post-seismic monitoring of cliff mass wasting using an unmanned aerial vehicle and field data at Egremni Lefkada Island Greece. Geomorphology 367:107306
Koukouvelas IK, Piper DJW, Katsonopoulou D, Kontopoulos N, Verroios S, Zygouri V (2020b) Earthquake-triggered landslides and mudflows: was this the wave that engulfed Ancient Helike? Holocene 30(12):1653–1668
Li HB, Qi SC, Chen H, Liao HM, Cui YF, Zhou JW (2019) Mass movement and formation process analysis of the two sequential landslide dam events in Jinsha River Southwest China. Landslides 16:2247–2258
Li HB, Qi SC, Yang XG, Li XW, Zhou JW (2020) Geological survey and unstable rock block movement monitoring of a post-earthquake high rock slope using terrestrial laser scanning. Rock Mech Rock Eng 53:4523–4537
Li Y, Chen LX, Yin KL, Zhang Y, Gui L (2021) Quantitative risk analysis of the hazard chain triggered by a landslide and the generated tsunami in the Three Gorges Reservoir area. Landslides 18:667–680
Liu SZ, Zhang LY (1994) Interpretation of satellite image and preliminary research on Danba whirl structure. Remote Sens Land Resour 21:25–33 (in Chinese)
Martha TR, Roy P, Govindharaj KB, Kumar KV, Diwakar PG, Dadhwal VK (2015) Landslides triggered by the June 2013 extreme rainfall event in parts of Uttarakhand state India. Landslides 12:135–146
Samodra G, Hadmoko DS, Wicaksono GN, Adi IP, Yudinugroho M, Wibowo SB, Suryatmojo H, Purwanto TH, Widartono BS, Lavigne F (2018) The March 25 and 29 2016 landslide-induced debris flow at Clapar Banjarnegara, Central Java. Landslides 15:985–993
Setiawan H, Wilopo W, Wiyoso T, Fathani TF, Karnawati D (2019) Investigation and numerical simulation of the 22 February 2018 landslide-triggered long-traveling debris flow at Pasir Panjang Village Brebes Regency of Central Java Indonesia. Landslides 16:2219–2232
Shen DY, Shi ZM, Peng M, Zhang LM, Zhu Y (2021) Preliminary analysis of a rainfall-induced landslide hazard chain in Enshi City Hubei Province China in July 2020. Landslides 18:509–512
Tacconi Stefanelli C, Vilímek V, Emmer A, Catani F (2018) Morphological analysis and features of the landslide dams in the Cordillera Blanca Peru. Landslides 15:507–521
Tuozzolo S, Lind G, Overstreet B, Mangano J, Fonstad M, Hagemann M, Frasson RD, Larnier K, Garambois PA, Monnier J, Durand M (2019) Estimating river discharge with swath altimetry: a proof of concept using AirSWOT observations. Geo Res Lett 46(3) 1459–1466. https://doi.org/10.1029/2018GL080771
Wang LJ, Chang M, Dou XY, Ma GH, Yang CY (2017) Analysis of river blocking induced by a debris flow. Geofluids 2017:1268135
Yang F, Feng Z, Liu M, Fan X (2020) Prediction of a multi-hazard chain by an Integrated numerical simulation approach: the Baige landslide along the Jinsha River, China. In: Zhang JM, Zhang L, Wang R (eds) Dam Breach Modelling and Risk Disposal ICED 2020 Springer Series in Geomechanics and Geoengineering. Springer, Cham, pp 383–392
Yu F (2018) Development characteristics cause analysis and control study of debris flow in Danba County. Southwest Jiaotong University, Chengdu (Master Degree Thesis, In Chinese)
Zhou JW, Cui P, Hao MH (2016) Comprehensive analyses of the initiation and entrainment processes of the 2000 Yigong catastrophic landslide in Tibet China. Landslides 13:39–54
Zhou JW, Li HB, Lu GD, Zhou Y, Zhang JY, Fan G (2020a) Initiation mechanism and quantitative mass movement analysis of the 2019 Shuicheng catastrophic landslide. Q J Eng Geol Hydrogeol. https://doi.org/10.1144/qjegh2020-052
Zhou GD, Roque PJC, Xie YX, Song DR, Zou Q, Chen HY (2020b) Numerical study on the evolution process of a geohazards chain resulting from the Yigong landslide. Landslides 17:2563–2576
Zou Q, Su ZM, Zhu XH (2013) Mechanism of landslide-debris flow-dammed lake disaster chain after the Wenchuan earthquake. In: Ugai K, Yagi H, Wakai A (eds) Earthquake-Induced Landslides. Springer, Berlin Heidelberg, pp 917–924
Zygouri V, Koukouvelas IK (2018) Landslides and natural dams in the Krathis River north Peloponnese Greece. Bull Eng Geol Environ 78:207–222